ACS Catalysis

Letter

pubs.acs.org/acscatalysis

Ni–Mo Nanopowders for Efficient Electrochemical Hydrogen Evolution

James R. McKone, Bryce F. Sadtler, Caroline A. Werlang, Nathan S. Lewis, and Harry B. Gray*

Division of Chemistry and Chemical Engineering, the Kavli Nanoscience Institute, and the Beckman Institute, California Institute of Technology, 1200 E. California Blvd., Pasadena, California 91125, United States

Supporting Information

ABSTRACT: Earth-abundant metals are attractive alternatives to the noble metal composite catalysts that are used in water electrolyzers based on proton-exchange membrane technology. Ni–Mo alloys have been previously developed for the hydrogen evolution reaction (HER), but synthesis methods to date have been limited to formation of catalyst coatings directly on a substrate. We report a method for generating unsupported nanopowders of Ni–Mo, which can be suspended in common solvents and cast onto arbitrary substrates. The mass-specific catalytic activity under alkaline conditions approaches that of the most active reported non-noble HER catalysts, and the coatings display good stability under alkaline conditions. We have also estimated turnover frequencies per surface atom at various overpotentials and conclude that the activity enhancement for Ni–Mo relative to pure Ni is due to a combination of increased surface area and increased fundamental catalytic activity.

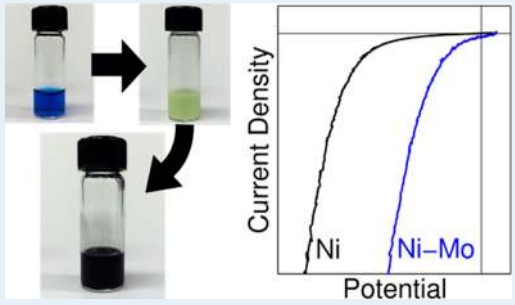

KEYWORDS: *nickel, molybdenum, Ni–Mo, hydrogen evolution, HER, cathode, electrolysis, stability*

Alkaline electrolysis is an attractive alternative to proton-exchange membrane (PEM)-based electrolysis because the non-noble metal electrocatalysts involved in alkaline electrolysis are stable and exhibit relatively high activity for both the hydrogen evolution reaction (HER) and the oxygen-evolution reaction (OER). Alkaline electrolyzers generally use Ni-based materials, or steel, as the electrodes and/or electrocatalysts.[1] Specifically, Ni–Mo alloys exhibit high activity and long-term stability as HER catalysts under alkaline conditions.[2−5] Ni–Mo composites have also recently been mixed with other elements, such as zinc or nitrogen, to provide enhanced HER activity and/or stability under neutral or acidic conditions.[6,7]

Electrocatalysts used in modern PEM-based fuel cell and electrolysis systems are generally synthesized as powders or colloids, and often supported on a porous, conductive matrix such as carbon black.[8,9] This mode of synthesis permits facile processing and attachment of the electrocatalyst to suitable substrates, such as metallic current-collectors or ion-exchange membranes. Synthesis of highly processable powders also facilitates assessment of the maximum attainable mass-specific catalytic activity of the electrocatalyst of interest. In contrast, the electrochemical behavior of Ni–Mo alloys has generally been investigated by the synthesis of the active electrocatalyst directly onto an electrode substrate,[2−5,10−20] confounding direct characterization of the morphology, composition, and activity of the electrocatalytically active species.

We describe a method for synthesizing unsupported Ni–Mo nanopowders that exhibit high catalytic activity for the HER. The powder is readily processed into colloidal inks and can be deposited in desired loadings onto substrates. The composition, morphology, catalytic activity, and stability during hydrogen evolution of such Ni–Mo nanopowders under aqueous acidic and alkaline conditions have been evaluated in detail.

A two-step precipitation/reduction process was used to prepare the Ni–Mo nanopowders (Figure 1; also see Supporting Information). First, an aqueous solution of nickel hexammine and ammonium molybdate was prepared at a 6:4 mol ratio of Ni to Mo. Then the mixture was rapidly heated in diethylene glycol, leading to precipitation of a green mixed Ni–Mo oxide powder. The oxide powder was recovered by centrifugation, dried, and subsequently reduced under forming

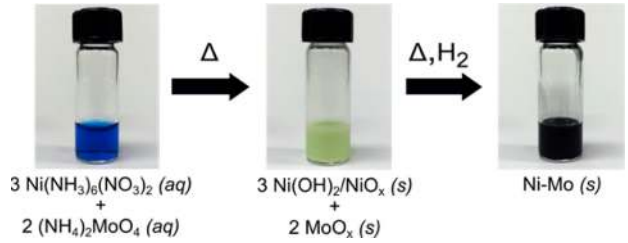

Figure 1. Synthetic scheme for generating Ni–Mo nanopowder, involving an initial precipitation step and subsequent heat treatment under a reducing atmosphere.

Received: October 26, 2012
Revised: November 30, 2012
Published: December 3, 2012

gas to generate a black Ni–Mo nanopowder. The initial precipitation was also successfully performed with water as the solvent, in which case the method closely resembled the synthesis of a known ammonium nickel molybdate.[21]

Figure 2 shows scanning electron microcope (SEM) and transmission electron microscope (TEM) images of the Ni–Mo oxide and Ni–Mo nanopowders. The Ni–Mo oxide exhibited a polydisperse nanoparticulate morphology, with particle sizes ranging from 50 to 300 nm. The oxide also exhibited low crystallinity by electron diffraction (Supporting Information). Upon reduction, the powder retained a nanoparticulate morphology, but exhibited increased crystallinity (Supporting Information) and porosity (Figure 2d). The increase in porosity is consistent with the volume contraction expected upon reduction of the oxidized intermediate to the putatively metallic Ni–Mo product. Energy dispersive spectroscopic analysis integrated in the SEM indicated that, for powders that had ≤40% Mo content, the Ni:Mo atomic ratios in the powders generally were in accord with the Ni:Mo atomic ratios in the precursor solutions. For precursor solutions with >40% Mo content, however, the resulting catalyst contained a lower proportion of Mo than the precursor solution (Supporting Information).

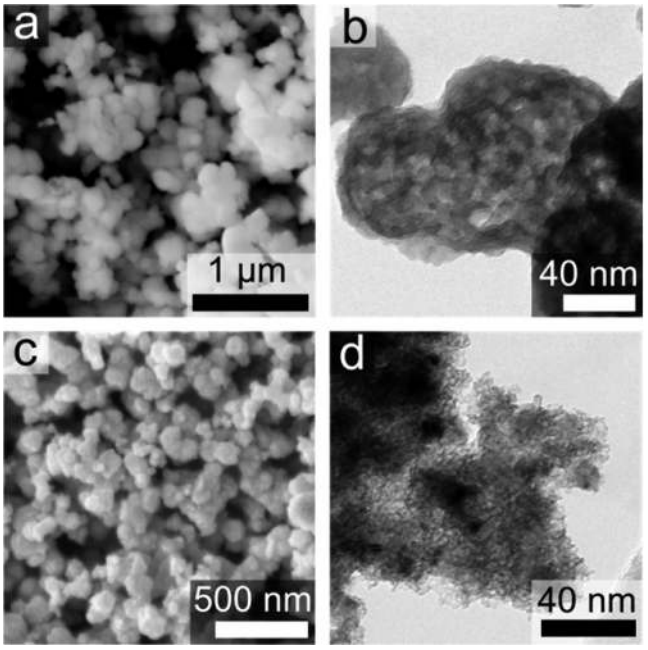

Figure 2. Scanning electron micrographs (left) and transmission electron micrographs (right) of Ni–Mo oxide intermediate (a,b) and Ni–Mo nanopowders (c,d).

The hydrogen evolution activity and electrochemical stability of these Ni–Mo nanopowders were evaluated under alkaline and acidic conditions by dispersing the Ni–Mo in isopropanol followed by deposition of the particles onto clean Ti electrodes. The highest catalytic activities were observed after a second reduction step had been performed on the deposited films, presumably because of the tendency of the nanopowders to form surface oxides in air. Indeed, the powders were pyrophoric in air, and were generally kept wet with water or solvent until catalytic films were generated.

Figure 3 shows the room temperature polarization data under alkaline conditions for various catalysts, including films of Ni–Mo nanopowders on Ti. For Ni–Mo loadings of 1 mg cm^{-2}, <100 mV overpotential, η, was required to sustain cathodic current densities in excess of 10 mA cm^{-2}. These activities greatly exceeded those exhibited by the Ti substrate, by smooth Ni electrodes, or by Ni nanopowder films that had been generated by the same precipitation-reduction. Ni–Mo films exhibited similarly high catalytic activities under alkaline conditions for Mo contents ranging from 10 to 50% (Supporting Information).

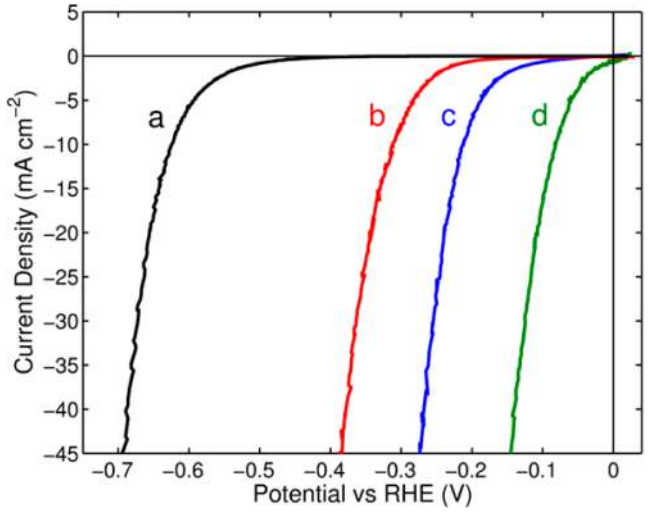

Figure 3. Comparison of HER catalytic activities for various electrodes in 1 M NaOH solution. The counter electrode was a Ni mesh, and the reference was Hg/HgO (1 M NaOH). Potentials are reported versus the thermodynamic potential for hydrogen evolution, which was measured after the experiments using a clean Pt electrode. The data are labeled as follows: (a) Ti foil substrate; (b) Smooth Ni wire; (c) Ni nanopowder on Ti foil (1 mg cm^{-2}); (d) Ni–Mo nanopowder on Ti foil (1 mg cm^{-2}).

The stability of the deposited Ni–Mo electrocatyst films was evaluated under acidic and alkaline conditions by galvanostatic control of the electrodes at a current density $J = -20$ mA cm^{-2} (Figure 4). Under alkaline conditions, the overpotential at $J = -20$ mA cm^{-2} was stable for 100 h, and in fact η decreased

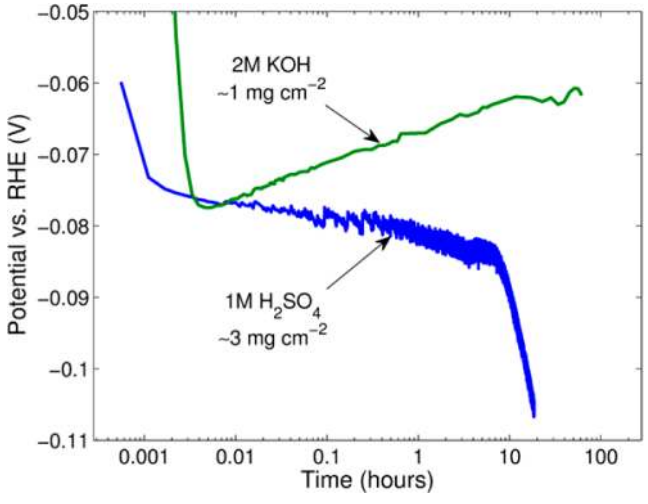

Figure 4. Potential vs log(time) plot for Ni–Mo nanopowder films on Ti electrodes with the noted mass loadings in the noted electrolytes. Electrodes were poised galvanostatically at −20 mA cm^{-2}.

dx.doi.org/10.1021/cs300691m | ACS Catal. 2013, 3, 166–169

Table 1. Collected HER Catalysis Data

catalyst	loading (mg cm^{-2})	electrolyte	temperature (°C)	η (mV)	J (mA cm^{-2})	reference
Ni−Mo nanopowder	1.0	2 M KOH	25	70	20	this work
Ni−Mo nanopowder	3.0	0.5 M H_2SO_4	25	80	20	this work
Ni−Mo nanopowder	13.4	2 M KOH	25	100	130	this work
Ni−Mo on Ni	20	30 wt % KOH	70	80	1000	Brown and Mahmood[5]
Ni−Mo on Ni	40	1 M KOH	40	110	400	Xiao, et al.[23]
Ni−Mo nitride nanosheets	0.25	0.1 M $HClO_4$	25	200	3.5	Chen, et al.[6]
Pt on Carbon	0.28	0.5 M H_2SO_4	25	50	20	Li, et al.[24]
amorphous MoS_x	(10^{17} sites cm^{-2})	0.5 M H_2SO_4	25	200	10	Benck, et al.[25]
MoS_2 on reduced graphene oxide	0.28	0.5 M H_2SO_4	25	150	10	Li, et al.[24]
MoS_x on graphene-coated Ni foam	8	0.5 M H_2SO_4	25	200	45	Chang, et al.[26]

approximately linearly with log(time) over the time period. This aging effect, which has been observed previously, was attributed to the dissolution of residual molybdenum not incorporated into an alloy phase in the electrocatalyst.[2,4]

Under acidic conditions, the η required to pass −20 mA cm^{-2} was also initially <100 mV. However, in acid, η increased (linearly) with log(time), and the performance degraded rapidly after ∼7 h under galvanostatic conditions. This behavior is in accord with expectations for a continuous, slow corrosion of the catalyst coating, which eventually led to dissolution of a large fraction of the electrocatalytic material. Greatly enhanced stability in acidic media has been reported recently for Ni−Mo materials mixed with carbon and nitrogen,[6] albeit at much higher overpotentials to obtain similar J values to those reported herein. The hydrogen evolution activity data for this and several recently reported catalyst systems are compared in Table 1.

Figure 5 shows the current densities produced at constant overpotentials of 100 and 200 mV, respectively, by various Ni−Mo loadings on Ti. The relationship between the mass loading and the current density was well described by a power law, for example, $J = -14.45m^{0.86}$ at η = 100 mV, where J is the current density in mA cm^{-2} and m is the mass loading in mg cm^{-2} (blue line in Figure 5). The observed power law is consistent

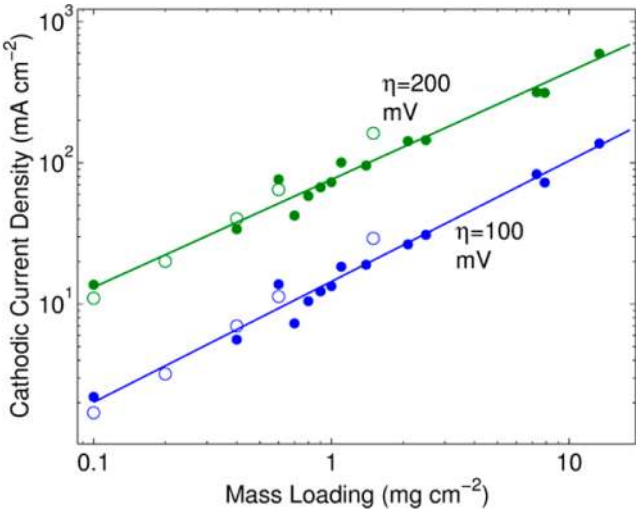

Figure 5. Current density versus mass loading (log−log plot) for Ti substrates coated with various quantities of Ni−Mo nanopowder at the noted overpotentials in 2 M KOH solution. The associated lines are fit to the data by power laws attributed to attenuation of increased catalytic activity with increased mass loading. Open and closed circles are data from two different sets of electrodes.

with attenuation of the marginal increase in activity with increased mass loading due to diminished transport of reactant species through porous films of increasing thickness.

For comparison, current densities J = −1000 mA cm^{-2} have been observed at η = 80 mV for highly optimized Ni−Mo electrodes at ∼20 mg cm^{-2} mass loading and at 70 °C in 30 wt % KOH(aq).[5] The mesh geometry, electrolyte concentration, and increased temperature presumably all contributed to the very high observed activity for this Ni−Mo cathode. In the present system, mass loadings >10 mg cm^{-2} were difficult to obtain because of poor adhesion of such nanoparticle films to the Ti substrate. The adhesion could likely be improved, however, by the use of polymer binders or mesh substrates that have similar surface redox chemistry and thermal expansion characteristics as the catalytic coating.

Measurement of mass-specific catalytic activities enables an estimation of the activity of Ni−Mo nanopowders on a per-surface-atom basis, given a series of approximations regarding particle composition and morphology. The total surface area of 0.1 mg of spherical, 5 nm diameter particles with a density of 9.5 g mol^{-1} (based on the weighted-average density of 6:4 Ni/Mo metals) is ∼130 cm^2, implying that the roughness factor, γ, for a 0.1 mg cm^{-2} sample is ∼130. Assuming that the nanoparticle surfaces exhibit the weighted-average lattice constants of their bulk Ni and Mo components, 0.1 mg of material contains 0.4 μmol of surface atoms. Hence for films with low mass loading, the turnover frequencies can be estimated as 0.05 s^{-1} at η = 100 mV and 0.36 s^{-1} at η = 200 mV.[22]

Commercially available samples of pure Ni, as well as of metallurgically prepared Ni−Mo alloys with Mo loadings of 1, 4, and 12%, respectively, were also evaluated electrochemically for their activities toward the HER. Samples of these materials were cut and polished to produce a smooth surface, chemically etched to remove surface polishing damage (Supporting Information), and tested for electrocatalytic hydrogen evolution activity under alkaline conditions (Figure 6). The data showed a clear monotonic trend, in which increasing Mo loading resulted in decreased overpotentials required to obtain a specified current density. Notably, assuming surface roughness factors of 1, the data for 0 and 12% Mo imply turnover frequencies at η = 100 mV of 0.03 and 0.2 s^{-1} per surface atom, respectively. These values are within an order of magnitude of those estimated for the Ni−Mo nanopowders, and support the notion that alloying Mo into Ni increases the fundamental hydrogen evolution activity of Ni metal. This further implies that both enhanced fundamental reactivity and increased surface area are operative in the observed catalytic activity of Ni−Mo nanopowder.

dx.doi.org/10.1021/cs300691m | ACS Catal. 2013, 3, 166−169

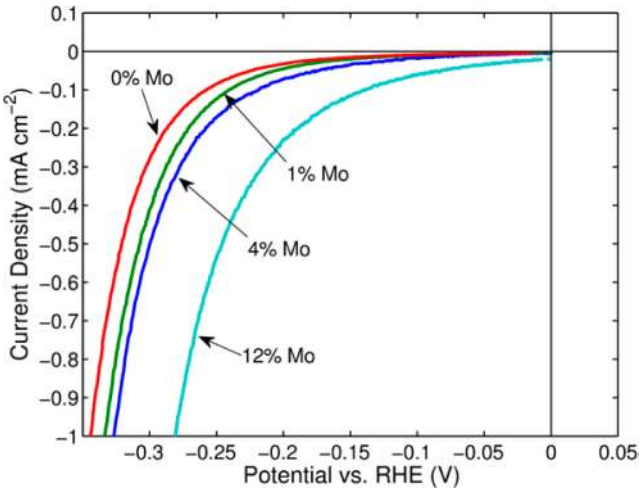

Figure 6. Room-temperature polarization data of metallurgically prepared Ni and Ni−Mo alloys with varying Mo content. Experiments were performed in 2 M KOH solution.

In conclusion, unsupported nanopowders of Ni−Mo alloy can be readily prepared and processed into films that have various mass loadings. The resulting non-noble electrocatalysts exhibit high mass-specific activities for the HER under alkaline conditions. The coatings are very stable under hydrogen evolution conditions in alkaline electrolytes, but degrade after operation for a few hours under acidic conditions. The exceptionally high activity is due in part to high porosity in the films, but Ni−Mo nanopowders also exhibit enhanced per-surface-atom activity as compared with Ni, as corroborated by electrochemical polarization measurements on well-defined samples of metallurgical alloys.

■ ASSOCIATED CONTENT

Supporting Information

Materials, synthetic methods, and characterization details are included as Supporting Information. Additionally included is a spreadsheet (Excel format) demonstrating the calculations for turnover frequency per surface atom. This material is available free of charge via the Internet at http://pubs.acs.org.

■ AUTHOR INFORMATION

Corresponding Author

*E-mail: hbgray@caltech.edu.

Notes

The authors declare no competing financial interest.

■ ACKNOWLEDGMENTS

This work was supported by the National Science Foundation "Powering the Planet" Center for Chemical Innovation (CHE-0802907). We thank Carol M. Garland for assistance with transmission electron microscopy. J.R.M. acknowledges the Department of Energy, Office of Science for a graduate research fellowship. C.A.W. thanks the Caltech Summer Undergraduate Research Fellowship (SURF) program for support during the summer of 2012. B.F.S. acknowledges the Beckman Institute for a postdoctoral fellowship.

■ REFERENCES

(1) Trasatti, S. In *Advances in Electrochemical Science and Engineering*; Gerischer, H., Tobias, C. W., Eds.; VCH: Weinheim, Germany, 1992; Vol. *2*, p 1.
(2) Brown, D. E.; Mahmood, M. N.; Man, M. C. M.; Turner, A. K. *Electrochim. Acta* **1984**, *29*, 1551.
(3) Brown, D. E.; Mahmood, M. N.; Turner, A. K.; Hall, S. M.; Fogarty, P. O. *Int. J. Hydrogen Energy* **1982**, *7*, 405.
(4) Stachurski, J. Z. O.; Pouli, D.; Ripa, J. A.; Pokrzyk, G. F. U.S. Patent 4,354,915, 1982.
(5) Brown, D. E.; Mahmood, M. N. U.S. Patent 4,358,475, 1982.
(6) Chen, W.-F.; Sasaki, K.; Ma, C.; Frenkel, A. I.; Marinkovic, N.; Muckerman, J. T.; Zhu, Y.; Adzic, R. R. *Angew. Chem., Int. Ed.* **2012**, *51*, 6131.
(7) Nocera, D. G. *Acc. Chem. Res.* **2012**, *45*, 767.
(8) Mehta, V.; Cooper, J. S. *J. Power Sources* **2003**, *114*, 32.
(9) Litster, S.; McLean, G. *J. Power Sources* **2004**, *130*, 61.
(10) Raj, I. A.; Venkatesan, V. K. *Int. J. Hydrogen Energy* **1988**, *13*, 215.
(11) Divisek, J.; Schmitz, H.; Balej, J. *J. Appl. Electrochem.* **1989**, *19*, 519.
(12) Huot, J. Y.; Trudeau, M. L.; Schulz, R. *J. Electrochem. Soc.* **1991**, *138*, 1316.
(13) Raj, I. A. *J. Mater. Sci.* **1993**, *28*, 4375.
(14) Fan, C.; Piron, D. L.; Sleb, A.; Paradis, P. *J. Electrochem. Soc.* **1994**, *141*, 382.
(15) Hu, W. K.; Cao, X. J.; Wang, F. P.; Zhang, Y. S. *Int. J. Hydrogen Energy* **1997**, *22*, 621.
(16) Kawashima, A.; Akiyama, E.; Habazaki, H.; Hashimoto, K. *Mater. Sci. Eng., A* **1997**, *226*, 905.
(17) Hu, C. C.; Weng, C. Y. *J. Appl. Electrochem.* **2000**, *30*, 499.
(18) Navarro-Flores, E.; Chong, Z.; Omanovic, S. *J. Mol. Catal. A: Chem.* **2005**, *226*, 179.
(19) Krstajic, N.; Jovic, V.; Gajic-Krstajic, L.; Jovic, B.; Antozzi, A.; Martelli, G. *Int. J. Hydrogen Energy* **2008**, *33*, 3676.
(20) Han, Q.; Cui, S.; Pu, N.; Chen, J.; Liu, K.; Wei, X. *Int. J. Hydrogen Energy* **2010**, *35*, 5194.
(21) Levin, D.; Soled, S. L.; Ying, J. Y. *Inorg. Chem.* **1996**, *35*, 4191.
(22) This estimation method is sensitive to the aforementioned approximations, especially that of nominal particle size. However, it is comparatively insensitive to the relative proportion of Ni and Mo. See Supporting Information for full details.
(23) Xiao, L.; Zhang, S.; Pan, J.; Yang, C.; He, M.; Zhuang, L.; Lu, J. *Energy Environ. Sci.* **2012**, *5*, 7869.
(24) Li, Y.; Wang, H.; Xie, L.; Liang, Y.; Hong, G.; Dai, H. *J. Am. Chem. Soc.* **2011**, *133*, 7296.
(25) Benck, J. D.; Chen, Z.; Kuritzky, L. Y.; Forman, A. J.; Jaramillo, T. F. *ACS Catal.* **2012**, *2*, 1916.
(26) Chang, Y.-H.; Lin, C.-T.; Chen, T.-Y.; Hsu, C.-L.; Lee, Y.-H.; Zhang, W.; Wei, K.-H.; Li, L.-J. *Adv. Mater.* **2012**, in press.